THE JOURNAL OF BIOLOGICAL CHEMISTRY VOL. 284, NO. 28, pp. 18980–18993, July 10, 2009


# Clarin-1, Encoded by the Usher Syndrome III Causative Gene, Forms a Membranous Microdomain

## *POSSIBLE ROLE OF CLARIN-1 IN ORGANIZING THE ACTIN CYTOSKELETON*[*] [S]

Received for publication, April 2, 2009, and in revised form, April 22, 2009 Published, JBC Papers in Press, May 7, 2009, DOI 10.1074/jbc.M109.003160

**Guilian Tian**[‡1], **Yun Zhou**[‡1], **Dagmar Hajkova**[‡§], **Masaru Miyagi**[‡§], **Astra Dinculescu**[¶], **William W. Hauswirth**[¶], **Krzysztof Palczewski**[‡], **Ruishuang Geng**[‖], **Kumar N. Alagramam**[‖], **Juha Isosomppi**[**‡‡], **Eeva-Marja Sankila**[**§§], **John G. Flannery**[¶¶], **and Yoshikazu Imanishi**[‡2]

*From the* [‡]*Department of Pharmacology, Case Western Reserve University, Cleveland, Ohio 44106-4965, the* [§]*Case Center for Proteomics, Case Western Reserve University, Cleveland, Ohio 44106-4965, the* [¶]*Department of Ophthalmology, University of Florida, Gainesville, Florida 32610-0284, the* [‖]*Department of Otolaryngology Head & Neck Surgery, University Hospitals Case Medical Center, Case Western Reserve University, Cleveland, Ohio 44106-4965, the* [**]*Department of Molecular Genetics, Folkhälsan Institute of Genetics, FIN-00014 Helsinki, Finland, the* [‡‡]*Department of Medical Genetics, University of Helsinki, FIN-00014 Helsinki, Finland, the* [§§]*Department of Ophthalmology, University of Helsinki, FIN-00014 Helsinki, Finland, and the* [¶¶]*Helen Wills Neuroscience Institute, University of California, Berkeley, California 94720*

**Clarin-1 is the protein product encoded by the gene mutated in Usher syndrome III. Although the molecular function of clarin-1 is unknown, its primary structure predicts four transmembrane domains similar to a large family of membrane proteins that include tetraspanins. Here we investigated the role of clarin-1 by using heterologous expression and *in vivo* model systems. When expressed in HEK293 cells, clarin-1 localized to the plasma membrane and concentrated in low density compartments distinct from lipid rafts. Clarin-1 reorganized actin filament structures and induced lamellipodia. This actin-reorganizing function was absent in the modified protein encoded by the most prevalent North American Usher syndrome III mutation, the N48K form of clarin-1 deficient in *N*-linked glycosylation. Proteomics analyses revealed a number of clarin-1-interacting proteins involved in cell-cell adhesion, focal adhesions, cell migration, tight junctions, and regulation of the actin cytoskeleton. Consistent with the hypothesized role of clarin-1 in actin organization, F-actin-enriched stereocilia of auditory hair cells evidenced structural disorganization in *Clrn1*$^{-/-}$ mice. These observations suggest a possible role for clarin-1 in the regulation and homeostasis of actin filaments, and link clarin-1 to the interactive network of Usher syndrome gene products.**

Usher syndrome is the most common cause of human inherited deafness and blindness, accounting for ~50% of all cases (1). There are three clinical types of Usher syndrome, types I, II, and III (1–3). Usher type I is characterized by profound congenital deafness and vestibular dysfunction, and Usher type II is characterized by moderate to severe deafness. Usher type III is distinguished from types I and II by progressive (non-congenital) deafness together with variable impairment of vestibular function. All Usher types lead to progressive retinal degeneration with a retinitis pigmentosa-like appearance. Five causative genes have been identified for Usher syndrome type I, and three genes for type II (3). The protein products of Usher type I and II genes are functionally heterogeneous, including an unconventional myosin, scaffold proteins, G-protein-coupled receptor, and cadherins. Adding to this heterogeneity, the Usher syndrome type III gene encodes a novel transmembrane protein named clarin-1 (CLRN1)[3] (4–6) with an unknown function. The heterogeneity of genes involved in Usher syndrome makes it extremely challenging to elucidate shared and distinctive disease mechanisms.

CLRN1 belongs to a superfamily of four-transmembrane proteins that includes the tetraspanin and claudin families. CLRN1 and its paralogues, CLRN2 and CLRN3, form the Clarin family, which is conserved throughout vertebrate species and shows limited sequence homology to the tetraspanins (4). Tetraspanins are considered to be structural proteins that interact laterally with other membrane proteins such as ion channels, integrins, and other tetraspanins (7, 8) to form tetraspanin-enriched microdomains. Tetraspanin-enriched microdomains embody other proteins to allow localized transmission of signals, cell-cell adhesion/fusion, cell-matrix interactions, and/or formation of diffusion barriers against small molecules. Similar to tetraspanins, CLRN1 retains only limited hydrophilic

* This work was supported by the Hope for Vision Foundation and the Elden Foundation.
This work is dedicated to Cindy Elden.
[S] The on-line version of this article (available at http://www.jbc.org) contains supplemental Figs. S1–S3.
[1] Both authors contributed equally to this work.
[2] To whom correspondence should be addressed: Dept. of Pharmacology, School of Medicine, Case Western Reserve University, Wood Bldg., 10900 Euclid Ave, Cleveland, OH 44106-4965. Tel.: 216-368-5226; Fax: 216-368-1300; E-mail: yxi19@case.edu.

[3] The abbreviations used are: CLRN1, clarin-1 protein; *CLRN1*, human clarin-1 gene, mRNA or cDNA; *Clrn1*, mouse clarin-1 gene, mRNA or cDNA; CLRN1$^{N48K}$, human clarin-1 protein with Asn at position 48 replaced by Lys; *CLRN1*$^{N48K}$, human clarin-1 gene, mRNA or cDNA, with Asn at position 48 replaced by Lys; HA, influenza hemagglutinin; HEK293, human embryonic kidney 293 cell; mAb, monoclonal antibody; Me$\beta$CD, methyl-$\beta$-cyclodextrin; RPE, retinal pigmented epithelial; RT, reverse transcription; tet, tetracycline; PBS, phosphate-buffered saline; MES, 4-morpholineethanesulfonic acid; Bis-Tris, 2-[bis(2-hydroxyethyl)-amino]-2-(hydroxymethyl)propane-1,3-diol; PNGase F, peptide *N*-glycosidase F; Endo H$_f$, endoglycosidase H fused to maltose binding protein; P, postnatal day.

regions exposed to cytoplasmic or extracellular aqueous phases (Fig. 1*A*) and, apparently, lacks any functional domains. Although CLRN1 is structurally related and similar to tetraspanins, it is currently unknown whether CLRN1 can form specific microdomains. The question also remains as to what one or more functions CLRN1 microdomains serve if indeed they do exist.

CLRN1 is expressed in sensory hair cells (4) where it may interact with other co-existing Usher gene products or cellular machinery essential for the maintenance of these cells. Increasing evidence suggests that products of Usher type I and II genes form large networks of interacting proteins, and that F-actin plays a major role in organizing these networks (reviewed in Refs. 2, 9). The core of these networks is the Usher type IC gene product, Harmonin, which interacts directly with F-actin *in vitro* and stabilizes F-actin when it is expressed heterologously in HeLa cells (10). Harmonins retain multiple PDZ domains dedicated to interacting with products of Usher type I and type II genes (reviewed in Refs. 2, 9) and also serve as PDZ domain-based scaffolds to anchor Usher proteins to F-actin. A link between Usher gene products and actin-based organelles also has been established *in vivo*. In Usher syndrome I and II mouse models, the actin-enriched stereocilia are morphologically and functionally defective (11–14). Because the causative gene for Usher type III was identified more recently than those of Usher types I and II, little is known about the pathogenesis of Usher syndrome III. Epistatic interactions between Usher syndrome type IB and Usher syndrome III may suggest linkage among CLRN1, Myosin VIIa, and F-actin (15). Clinically, patients with the N48K *CLRN1* mutation have a rod and cone degenerative phenotype similar to Usher type IIA patients (16), suggesting a common pathological pathway for Usher types IIA and III. Despite the genetic and phenotypic characterization in humans, the molecular function of CLRN1 remains elusive, as well as its relationship and interaction with other Usher gene products. Therefore, identifying possible interactive partners of CLRN1 should improve understanding of the function of CLRN1 and the common pathological pathways of progressive hearing and vision loss in the Usher syndromes.

Here we investigated whether CLRN1 can form microdomains similar to the tetraspanin-enriched microdomain, and if so, what the function of such microdomains might be. Our studies indicate that CLRN1 forms membranous cholesterol-rich compartments on plasma membranes and interacts with and regulates the machinery involved in actin filament organization. To understand the pathogenesis of Usher syndrome, we asked whether and how the Usher syndrome III causative mutation, N48K, results in dysfunction of the clarin-1-enriched microdomains involved in organizing actin. To determine whether Clrn1 is involved in the regulation of actin cytoskeleton *in vivo*, we studied the structure of F-actin-enriched stereocilia bundles in *Clrn1*$^{-/-}$ mouse. Because actin provides important scaffolds in Usher interactome, the observations described herein provide a novel molecular link between CLRN1 and the identified gene products of Usher types I and II.

## EXPERIMENTAL PROCEDURES

*Reagents*—Methyl-$\beta$-cyclodextrin (Me$\beta$CD), puromycin, Brij-58 (catalogue no.: P5884), Brij-96V (catalogue no.: 16011), Brij-98 (catalogue no.: P5641), and Igepal CA-630 (catalogue no.: I8896) were obtained from Sigma-Aldrich. EZ-Link Sulfo-NHS-SS-biotin, immobilized NeutrAvidin, and SuperSignal West Pico chemiluminescent substrate were obtained from Pierce. Complete protease inhibitor mixture was from Roche Applied Science. Mouse monoclonal antibody (mAb) anti-CLRN1 (clone 10B5) was raised against the C-terminal of mouse CLRN1 (TKSKETETTNVASDLMY). For several immunocytochemical experiments, anti-CLRN1 IgG was labeled with Cy3 by Amersham Biosciences Cy3 Mono-Reactive Dye Pack (Amersham Biosciences) following the manufacturer's instructions. Goat anti-actin polyclonal antibody was from Santa Cruz Biotechnology (Santa Cruz, CA). Mouse mAb anti-Flotillin-1 was from BD Transduction Laboratories (San Jose, CA). Mouse mAb anti-human transferrin receptor was from Zymed Laboratories Inc. (South San Francisco, CA). Mouse mAb anti-HA was from Covance. Mouse mAb anti-integrin $\beta$1 (clone P2D5), mouse mAb anti-tubulin (clone E7), and mouse mAb anti-ATPase($Na^+/K^+$)$\alpha$5 were obtained from the Developmental Studies Hybridoma Bank at University of Iowa (Iowa City, IA). Anti-N-cadherin (clone 13A9) and anti-$\alpha$-catenin (clone 1G5) (17, 18) were generous gifts from Dr. Emhonta Johnson (Dept. of Pharmacology, Case Western Reserve University). Unless otherwise stated, all other reagents were purchased from Fisher Scientific or Sigma-Aldrich.

*Cloning of CLRN1 cDNA*—The coding region of CLRN1 (NM_174878) was amplified from Human Retina Quick-Clone™ cDNA library (Clontech) with primers 5′-GTTTCTCATCATGCCAAGCCAACAGAAG-3′ and 5′-GTGACCAAAGCAAGTCTACTCCCTTGTA-3′, and cloned into a pCRII-TOPO vector (Invitrogen). A mammalian expression vector with a C-terminal HA tag was constructed by PCR amplification of CLRN1 from the pCRII-TOPO vector using primers 5′-TCTGCAGGCACCGTCGTCGACTTAACAGATCTCGATGCCAAGCCAA-3′ and 5′-TTAAGCGTAATCCGGAACATCGTATGGGTAGTACATTAGATCTGCAGCTA-3′, and then by recombining the construct into the phCMV3 Xi cloning vector (Gene Therapy Systems, Inc., San Diego, CA). Mutant cDNA construct representing p.N48K was generated by the QuikChange site-directed *in vitro* mutagenesis kit (Stratagene, La Jolla, CA).

*CLRN1 Expression Constructs*—Constructs were designed to express CLRN1 and its N48K mutant protein (CLRN1$^{N48K}$), each of them fused to HA and FLAG epitopes. PCR was performed with Phusion™ high fidelity polymerase (New England Biolabs, Ipswich, MA) to clone *CLRN1* cDNA into the corresponding expression vectors. The PCR conditions were: 98 °C for 30 s, 30 cycles of 98 °C for 10 s, 70 °C for 20 s, and 72 °C for 15 s. For stable expression, *CLRN1* and N48K mutant cDNA (*CLRN1*$^{N48K}$) were amplified by a pair of primers, 5′-CCGCTCGAGGCCACCATGCCAAGCCAACAGAAGAAAATC-3′ and 5′-CCGGAATTCTTACTTGTCGTCATCGTCTTTGTAGTCAGCGTAATCCGGAACATCGTATG-3′, by using cDNAs encoding CLRN1 and CLRN1$^{N48K}$ fused to the HA

epitope as templates (see the above section "Cloning of CLRN1 cDNA"). The PCR products were cloned into EcoR I and XhoI sites of MSCV puro vector (Clontech, Mountain View, CA). For inducible expression, *CLRN1* cDNA fused to HA epitope was amplified by a pair of primers, 5′-CGCGGATCCGCCACCATGCCAAGCCAACAGAAGAAAATC-3′ and 5′-CCCAAGCTTACTTGTCGTCATCGTCTTTGTAGTCAGCGTAATCCGGAACATCGTATG-3′, and then cloned into BamHI and HindIII sites of the vector pLP-RevTRE Acceptor Vector (Clontech) to obtain the inducible expression construct named pLP-RevTRE-*CLRN1*.

*Stable and Inducible Expression of CLRN1 in HEK293 Cells*—To establish stable expression of CLRN1, packaging PT67 cells were first transfected with MSCV CLRN expression vectors (see above) by using the Calcium Phosphate Transfection Kit (Invitrogen) following the manufacturer's instructions. Forty-eight hours after transfection, viruses were harvested by filtering the medium through a 0.45-$\mu$m filter (Millipore, Billerica, MA). Polybrene was added to the supernatant to a final concentration of 5 $\mu$g/ml. Human embryonic kidney 293 (HEK293) cells were incubated with viral supernatants at 37 °C in a $CO_2$ cell culture incubator. Forty-eight hours after infection, medium was replaced with fresh medium containing 1 $\mu$g/ml puromycin for positive selection of cells containing the *CLRN1* construct. Selection medium was replaced every 3 days until colonies formed 18–21 days later. Obtained stable cells were named HEK-CLRN for wild-type CLRN1, and HEK-CLRN$^{N48K}$ for mutant CLRN1$^{N48K}$.

To establish inducible expression of CLRN1, we first obtained a cell line that stably expressed a tet-responsive transcriptional activator. Retroviral supernatants collected from packaging PT67 cells transfected with pTet-on vector (Clontech) were used to infect HEK293 cells. 400 $\mu$g/ml G418 was used for selection over 2 weeks to obtain the HEK293 Tet-On cell line. Then retroviral supernatants were collected from PT67 cells transfected with pLP-RevTRE-*CLRN1* and used to infect the recipient HEK293 Tet-On cell line to obtain HEK-CLRN-ind cells. The selection method was similar to the one used for the stable cell lines, but 200 $\mu$g/ml hygromycin was included in the medium instead of puromycin. In all the stable and induced cells, CLRN1 expression was examined by immunocytochemistry and immunoblotting with mouse mAb anti-HA employed as the primary antibody.

*Cell Surface Biotinylation*—Proteins on the plasma membrane were labeled by biotinylation as described previously (19). Briefly, cells were incubated with 1 mg/ml EZ-Link® Sulfo-NHS-SS-Biotin in PBS buffer (137 mM NaCl, 2.7 mM KCl, 10.1 mM $Na_2HPO_4$, 1.8 mM $KH_2PO_4$, pH 7.4, 100 $\mu$M $CaCl_2$, and 1 mM $MgCl_2$) for 30 min at 4 °C. Then 100 mM glycine was added to react with excess biotin conjugate, and the incubation continued for another 30 min at 4 °C. Cells were lysed with 1% Triton X-100, and biotinylated proteins were recovered by incubation with 100 $\mu$l of immobilized NeutrAvidin at 4 °C overnight with end-over-end rotation. Loaded avidin beads were re-suspended in 1× SDS-PAGE loading buffer.

*Cholesterol Depletion*—HEK-CLRN cells were washed twice with PBS, and treated with 20 mM Me$\beta$CD in PBS at 37 °C in a $CO_2$ cell culture incubator for 30 min. After treatment, Me$\beta$CD solution was removed, and cells were harvested in PBS for further analysis.

*Discontinuous Sucrose Density Gradient Centrifugation*—Detergent-resistant microdomains were isolated by discontinuous sucrose density gradient centrifugation as described previously (20) with modifications. Briefly, HEK-CLRN cells were sonicated in sample buffer (320 mM sucrose in 50 mM Tris-HCl, pH 7.4), and centrifuged for 10 min at 1000 × *g* and 4 °C; collected supernatants were centrifuged for 15 min at 22,000 × *g* and 4 °C. Resulting pellets were lysed in buffer (150 mM NaCl, 25 mM MES, and complete protease inhibitor mixture, pH 6.5) containing either 1% (v/v) Triton X-100, 1% (v/v) Brij-35, 1% (v/v) Brij-96, 0.5% (v/v) Brij-98, or mixture of 1% (v/v) Igepal and 0.5% (v/v) sodium deoxycholate. After a 60-min incubation at 4 °C, sucrose was added to samples to reach a final concentration of 40% (w/v). One milliliter of each sample was overlaid with 2 ml of 30% (w/v) sucrose, and then with 1 ml of 5% (w/v) sucrose. Resulting samples were centrifuged for 16 h at 200,620 × *g* at 4 °C in a MLS-50 rotor (Beckman Coulter, Fullerton, CA). Ten 400-$\mu$l fractions were collected from the top to the bottom of the gradient for each experiment.

*Western Blots*—HEK-CLRN or HEK-CLRN$^{N48K}$ cells were grown in 10-cm dishes and lysed in 300 $\mu$l of buffer containing 10 mM Bis-Tris propane, 20 mM *n*-dodecyl-$\beta$-D-maltopyranoside (catalogue no.: D310S, Anatrace, Maumee, OH), 150 mM NaCl, 1 mM dithiothreitol (catalogue no.: 161-0610, Bio-Rad), 1 mM EDTA, 1 mM EGTA, 0.2 mM benzamidine, 0.5 mM phenylmethylsulfonyl fluoride (catalogue no.: 10837091001, Roche Applied Science), and protease inhibitor mixture (catalogue no.: 11836153001, Roche Applied Science). Cell lysates were incubated at 4 °C for 1 h and centrifuged at 14,000 rpm for 1 h. Protein quantities were normalized by the Bio-Rad protein assay (Bio-Rad). Samples were separated by 10% SDS-PAGE and then transferred to polyvinylidene difluoride membranes (Bio-Rad). Primary mouse mAb anti-HA was used to detect human CLRN1 and CLRN1$^{N48K}$ on these membranes. For detection of chemiluminescent signals, blot membranes were reacted with either anti-mouse or anti-rabbit IgG conjugated to horseradish peroxidase (Santa Cruz Biotechnology). Immunoreactive bands were detected by using the SuperSignal West Pico Chemiluminescent Substrate (Pierce) according to the manufacturer's directions. For colorimetric detection of signals, blot membranes were reacted with either anti-mouse or anti-rabbit IgG conjugated to alkaline phosphatase (Promega, Madison, WI), and immunoreactive bands were detected with the BCIP/NBT Color Development Substrate (Promega).

*Treatment of Cells with Tunicamycin, Doxycycline, and MG132*—HEK-CLRN or HEK-CLRN$^{N48K}$ cells were grown overnight to achieve 70% confluence, and cells were then treated with 5 $\mu$M MG132, a proteasome inhibitor. For induction of CLRN1 in HEK-CLRN-ind, cells were treated with 2 mM doxycycline. For inhibition of glycosylation, cells were treated with 1 $\mu$M tunicamycin 2 h prior to induction. For proteasome inhibition, cells were treated with 1.25 $\mu$M MG132 during CLRN1 induction. After induction, cells were cultured for 24 h. Cells were then either collected for Western blotting analysis by using HA antibody, or fixed for immunofluorescence imaging (see below).

*Glycosylation Analyses*—Protein samples prepared from HEK-CLRN or HEK-CLRN$^{N48K}$ cells as described above (see Western blot section) were treated with PNGase F (catalogue no.: P0704 S, New England Biolabs) or Endo $H_f$ (catalogue no.: P0703S, New England Biolabs). For PNGase F treatment, 15.5 $\mu$l of protein sample was mixed with 2.5 $\mu$l of 10× G7 reaction buffer, 2.5 $\mu$l of 10× glycoprotein denaturing buffer, 2.5 $\mu$l of 10% Nonidet P-40, and 2 $\mu$l of PNGase F enzyme, and the mixtures were incubated at room temperature for 3 h. For Endo $H_f$ treatment, 18 $\mu$l of protein sample was mixed with 2.5 $\mu$l of 10× G5 reaction buffer, 2.5 $\mu$l 10× glycoprotein denaturing buffer, and 2 $\mu$l of Endo $H_f$ and mixtures were incubated at room temperature for 3 h.

*Immunocytochemistry*—Cells or cross-sections of mouse eyecups were incubated with primary antibodies at 4 °C overnight. Signals were detected with either Cy3-conjugated secondary antibody (Jackson ImmunoResearch, West Grove, PA) or Alexa488-conjugated secondary antibody (Invitrogen). For several immunofluorescence studies, cells were double stained with two mouse mAbs. To avoid cross-reactivities between two mAbs, cells were first incubated with primary mouse anti-integrin, anti-catenin, or anti-N-cadherin mAb overnight at 4 °C and then probed with Alexa488-conjugated secondary antibody at room temperature for 1 h. Secondary antibodies then were blocked with the same primary antibodies for 1 h. After extensive washing, cells were incubated with Cy3-labeled 10B5 (mouse mAb anti-CLRN1) for 1 h. Samples were visualized by confocal microscopy.

*Whole Mount Preparation and Staining of Cochlear Hair Cell Stereocilia*—All animals studied were anesthetized and euthanized according to protocol approved by the Animal Care and Use Committee of the Case Western Reserve University. The basic protocol for this procedure was described previously (21). Briefly, mouse inner ears were dissected out from temporal bones at postnatal day 18 (P18). The round and oval windows of the cochlea were opened, and the apex was pierced with a fine needle. The cochlea was flushed with 4% paraformaldehyde in PBS (pH 7.5–8.0) and immersed in the fixative for 1 h at room temperature. After three washes in PBS the otic capsule was opened and the organ of Corti was dissected out in PBS at room temperature with a fine needle. Tissues were incubated with Alexa488-labeled phalloidin at 1:100 dilution in PBS containing 0.1% Triton (PBST) for 45 min at room temperature. After three washes with PBST for 5 min each, the hair cell stereocilia were visualized by confocal microscopy.

*Confocal Microscopy*—Samples were visualized with a TCS SP2 confocal microscope (Leica Microsystems Inc., Bannockburn, IL). Contrast and brightness of the images were adjusted by using Photoshop CS3 (Adobe Systems Inc., San Jose, CA). Only linear adjustments were applied.

*RT-PCR*—HEK-CLRN or HEK-CLRN$^{N48K}$ cells were grown first in 6-well plates to achieve 70% confluence. Total RNA was isolated by TRIzol (Invitrogen) according to the manufacturer's instructions. 5 $\mu$g of total RNA was treated by DNase I to digest DNA, and first strand cDNA was synthesized by using AffinityScript$^{TM}$ multiple temperature reverse transcriptase (Stratagene, catalogue no.: 600107) with oligo(dT18) as primer. Human *CLRN1* cDNA (696 bp) was amplified by primer pairs, 5′-ATGCCAAGCCAACAGAAG-3′ and 5′-GTACATTAGATCTGCAGCTAC-3′. PCR conditions were: 94 °C for 2 min; then 25 cycles of 94 °C for 30 s, 52 °C for 30 s, and 72 °C for 60 s. Glyceraldehyde-3-phosphate dehydrogenase was used as an internal control. Glyceraldehyde-3-phosphate dehydrogenase cDNA (240 bp) was amplified by using a pair of primers, 5′-TGATGACATCAAGAAGGTGGTGAAG-3′ and 5′-TCCTTGGAGGCCATGTGGGCCAT-3′. The PCR conditions were: 25 cycles of 94 °C for 30 s, 60 °C for 60 s, and 72 °C for 60 s.

For the studies of *Clrn1*$^{-/-}$ mice, cochleae collected from *Clrn1*$^{-/-}$ mice and *Clrn1*$^{+/+}$ littermates were homogenized, and total RNA was isolated by TRIzol. Fist strand cDNAs were synthesized by AffinityScript$^{TM}$ multiple temperature reverse transcriptase (Stratagene) by using a CLRN-specific primer C4 (5′-GTGGCCAAAGGAAGTCCATA-3′). β-Actin was used as an internal control with antisense primer 5′-TGTCAAAGAAAGGGTGTAAAACGCAGC-3′. CLRN1 DNA containing exons 1, 2, 3, and 4 was amplified by a primer set of C1 and C4 (C1 sequence: 5′-TTTACCGAAGCCTTTTCTCG-3′). Actin cDNA was amplified by primers 5′-CGGGACCTGACAGACTACCTCAT-3′ and 5′-TGTCAAAGAAAGGGTGTAAAACGCAGC-3′. PCR conditions were: 95 °C for 3 min; 35 cycles of 95 °C for 30 s, 55 °C for 30 s, and 72 °C for 1 min. RT-PCR product was cloned into pGEM®-T Easy vector (Promega) and sequenced.

*Affinity Purification of CLRN1*—HEK-CLRN cells were lysed in buffer (150 mM NaCl, 50 mM Tris, pH 8.0, and Complete protease inhibitor mixture) containing 1% (v/v) Brij-98 at 4 °C for 1 h, and centrifuged at 22,000 × *g* and 4 °C for 15 min. Collected supernatant was then loaded onto a discontinuous sucrose density gradient. The low density fractions containing CLRN1 were combined and incubated with EZview$^{TM}$ Red Anti-HA Affinity Gel at 4 °C overnight. The affinity gel was then spun down and washed four times with lysis buffer. Bound proteins then were eluted from the gel by 100 mM influenza hemagglutinin (HA) peptide in lysis buffer. Identical procedures were followed in control experiments, except the affinity gel was blocked by HA peptide before incubation with the low density fractions.

*Identification of CLRN1 Interacting Proteins*—Affinity-purified CLRN1-interacting proteins and proteins non-specifically bound to the resin were separated by SDS-PAGE by using NuPAGE® Novex 4–12% Bis-Tris gel (Invitrogen). Both lanes were cut into five gel bands and subjected to in-gel protein digestion with trypsin as described previously (22). Band 1 was from the top to 190 kDa, band 2 was from 190 to 75 kDa, band 3 was from 75 to 40 kDa, band 4 was from 40 to 30 kDa, and band 5 was from 30 kDa to the bottom. Resulting peptides from the CLRN1-interacting proteins and non-specifically bound proteins were labeled by $^{18}O$ and $^{16}O$, respectively, as described previously (23, 24), mixed in a 1:1 ratio, and desalted on a C18 column according to the manufacturer's manual. Mixed peptides were dissolved in 0.1% formic acid and analyzed by liquid chromatography-tandem mass spectrometry with an LTQ-Orbitrap mass spectrometer (Thermo Electron Corp., Bremen, Germany) (23).

Acquired data were subjected to Mascot search (version 2.2, Matrix Science, London, UK) against a Swiss-Prot v56 human

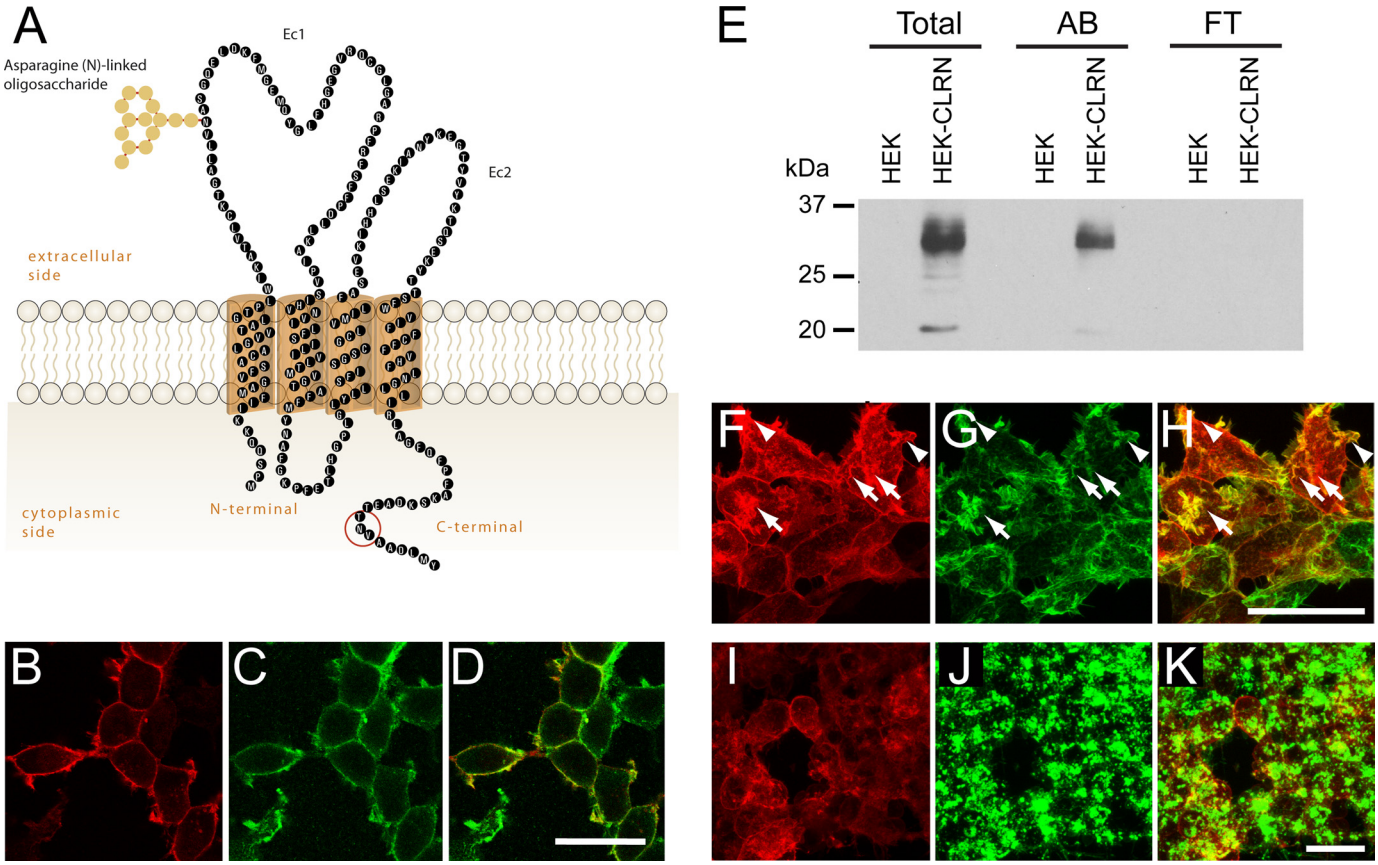


FIGURE 1. **CLRN1 is a plasma membrane protein localized at F-actin-enriched protrusions.** *A*, the topology and transmembrane domains shown were predicted with the HMMTOP transmembrane topology prediction server (55). The possible *N*-linked glycosylation site is indicated. Also shown (*red circle*) is the previously predicted motif near the CLRN1 C-terminal tail that may serve as a PDZ-binding site (4). *B*, immunolocalization of Human WT CLRN1. *C*, immunolocalization of Na/K ATPase in HEK293 cells stably expressing CLRN1. *D*, *merged image* of *B* and *C* indicates that CLRN1 and Na/K ATPase co-localize. *Images B–D* are single optical sections of HEK293 cells. *E*, cell surface biotinylation was performed to separate cell surface proteins (avidin-bound) (*AB*) from intracellular proteins (flow-through) (*FT*). Immunoblots of both fractions reveal that most of the CLRN1 protein localized to the plasma membrane. HEK293 cells alone and HEK293 cells expressing CLRN1 were preincubated for 30 min with Sulfo-NHS-SS-Biotin to label cell surface proteins. After cells were harvested, biotin-labeled CLRN1 protein levels were measured by immunoblotting. *F*, localization of human WT CLRN1 in HEK293 cells stably expressing CLRN1. *G*, F-actin in HEK293 cells stably expressing CLRN1. F-actins were labeled with phalloidin-Alexa 488. *H*, *merged image* of *F* and *G*. CLRN1 localized at both microvilli (*arrows*) and lamellipodia (*arrowheads*). *I–K*, CLRN1 localization studied by immunofluorescence confocal microscopy after disruption of F-actin by cytochalasin D treatment. *I*, CLRN1 localized diffusely on the plasma membrane. *J*, F-actin localization is shown. *K*, *merged image* of *I* and *J*. After disruption of F-actin, CLRN1 and F-actin no longer co-localize. Images *F–K* were generated from multiple optical sections by a maximum intensity projection. *Scale bars*, 50 $\mu$m.

data base to identify proteins. *S*-Carbamidomethylation of cysteine was set as a fixed modification. Oxidized methionines (methionine sulfoxide) with one or two C-terminal $^{18}O$ labels were set as variable modifications. Mass tolerance was set at 20 ppm for the precursor ion and to 1 Da for product ions. One miscleavage of trypsin was allowed. Custom built software, Relative Quantification O18.1.3.1, developed by Quanhu Sheng and Haixu Tang (University of Indiana, Bloomington, IN), was used to calculate $^{18}O/^{16}O$-labeled peptide and protein ratios. Proteins identified by at least two peptides with an ion score of 20 were considered for quantification.

*Scanning Electron Microscopy*—Methods used for scanning electron microscopy have been described previously (21, 25). Specimens from *Clrn1*$^{-/-}$ mice along with age-matched controls were studied by scanning electron microscopy.

## RESULTS

*CLRN1 Is a Plasma Membrane Protein*—The human *CLRN1* gene expresses a single, major mRNA isoform encoding a product of 232 amino acids. Moreover, all known disease-causing mutations are located in the coding region of this isoform. Although additional exons of the Usher syndrome type III gene were reported (6), expression of these exons was barely detectable by RT-PCR (5). Therefore, our study focused on the 232 amino acid isoform of CLRN1. CLRN1 is predicted to be an integral membrane protein with four transmembrane alpha helices (Fig. 1*A*). We found that CLRN1 localized to the plasma membrane when expressed in HEK293 cells. This was demonstrated by co-localization of CLRN1 with another plasma membrane protein, Na/K-ATPase (Fig. 1, *B–D*). Localization of CLRN1 was also studied biochemically. When HEK cells expressing CLRN1 were incubated with EZ-Link® Sulfo-NHS-SS-Biotin, most of the CLRN1 was found covalently conjugated to biotin (Fig. 1*E*). Because EZ-Link® Sulfo-NHS-SS-Biotin does not penetrate the plasma membrane, these biochemical observations prove that CLRN1 localizes on the plasma membrane with its hydrophilic parts exposed to the extracellular side. On the plasma membrane, CLRN1 was especially enriched in microvilli and lamellipodia (Fig. 1, *F–H*, *arrows* and *arrowheads*), as indicated by its co-localization with both phalloidin-

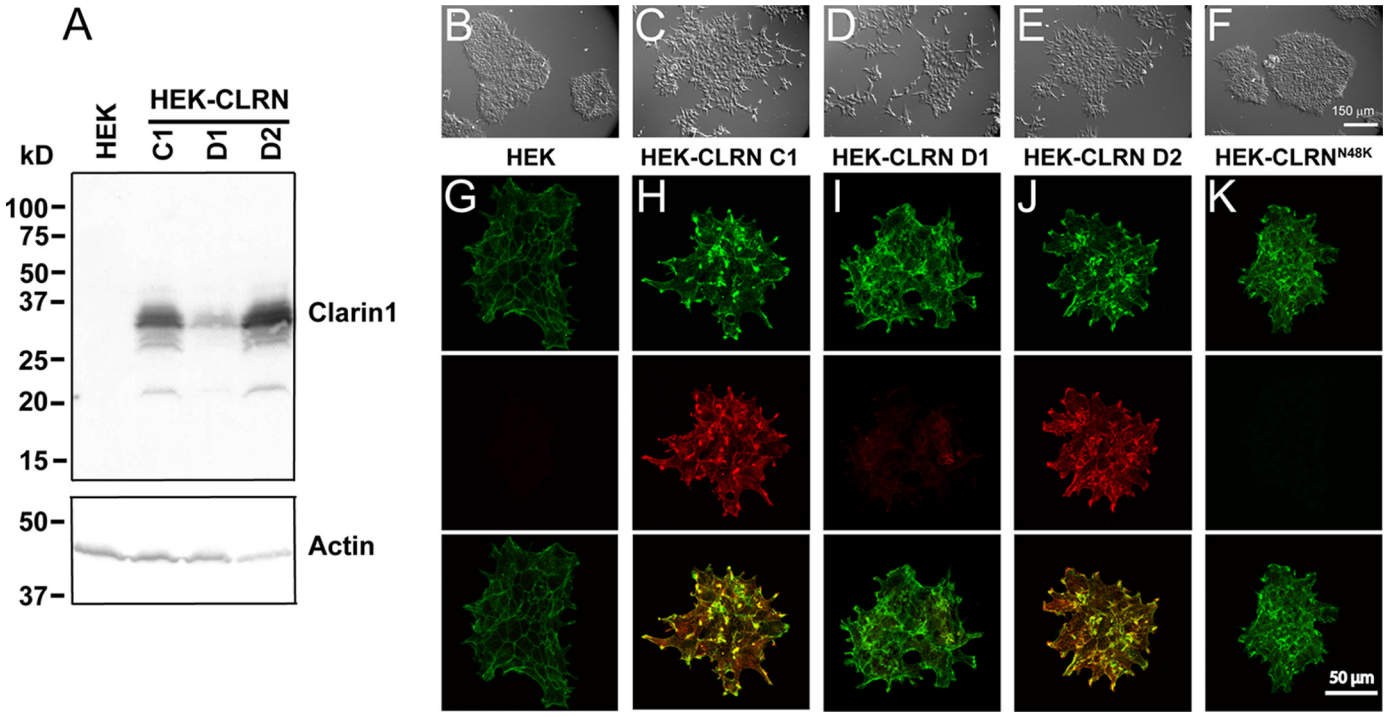


FIGURE 2. **CLRN1 induces reorganization of actin filaments and changes cellular morphology.** Here HEK293 cells stably expressing wild-type CLRN1 are indicated as HEK-CLRN C1, D1, and D2, and HEK 293 cells stably expressing the CLRN1$^{N48K}$ are indicated as HEK-CLRN$^{N48K}$. *A*, HEK-CLRN cell lines express different levels of CLRN1 protein. HEK293 and HEK-CLRN C1, D1, and D2 cells were lysed in 1% Igpal and 0.5% sodium deoxycholate, and CLRN1 was detected by immunoblotting with anti-Clarin-1 antibody 10B5. HEK293 cells did not show any detectable protein signals, whereas HEK-CLRN D2 cells expressed the highest levels of CLRN1 protein. *B–F*, HEK293 and stable cells expressing CLRN1 and CLRN1$^{N48K}$ were imaged by bright field microscopy. The cell line used for each experiment is indicated below each image. *Columns G–K*, HEK293 cells, HEK-CLRN cell lines, and HEK-CLRN$^{N48K}$ cells were imaged by confocal microscopy. Cells were labeled with Phalloidin-Alexa488 (*top row*, *green*) and anti-clarin-1 antibody 10B5 (*middle row*, *red*). The *bottom row* shows *merged images* from the *top* and *middle rows*. The cell line used for each experiment is indicated above each column. *Images G–K* were generated from multiple optical sections by a maximum intensity projection. Note: CLRN1 staining is weak in *I*, but the staining pattern is similar to *H* and *J*.

labeled F-actin, and the microvilli-enriched plasma membrane protein, Na/K-ATPase (Fig. 1, *B–D*) (26). Localization of CLRN1 was dependent on its interaction with F-actin, because disruption of F-actin led to diffuse localization of CLRN1 on the plasma membrane (Fig. 1, *I–K*).

*CLRN1 Induces Changes in Actin Organization and Motility of HEK293 Cells*—The possibility of interaction between CLRN1 and F-actin prompted a study of whether the overexpression of CLRN1 induces any remodeling of F-actin in HEK293 cells (Fig. 2). Three HEK-CLRN cell lines, C1, D1, and D2, that stably express human CLRN1 (Fig. 2*A*) were used to determine if CLRN1 expression affects the organization of actin filaments. HEK293 cells and human CLRN1 stable cell lines were plated on plastic dishes at low density so that colonies grew from single cells. Then, the proliferation and motility of cells in each colony were monitored (Fig. 2, *B–K*). Four days after plating, HEK293 cells had formed tightly packed colonies with round shapes (Fig. 2*B*), however, human CLRN1-stable cells were prone to form loosely packed colonies with ramifying lamellipodia (Fig. 2, *C–E*). During cellular proliferation and spreading, intense CLRN1 staining was observed at lamellipodia protrusions where actin filaments were highly concentrated (Fig. 2, *H–J*). Independently established stable cell clones showed similar phenotypes (Fig. 2, *C–E*) with the degree of this phenotype depending on the expression level of CLRN1 (Fig. 2*A*). For example, CLRN1 expression was higher in the C1 and D2 cell lines than in the D1 cell line (Fig. 2*A*) as were the amounts of F-actin at the cellular protrusions (Fig. 2, *H–J*). Without CLRN1 expression (Fig. 2*A* and supplemental Fig. S1*A*), HEK293 cells were far less prone to concentrate F-actin at cellular protrusions than in its presence (Fig. 2*G*). The CLRN1$^{N48K}$ mutant proteins failed to express at high levels in HEK293 cells, and as a result, did not promote changes in cellular morphology or F-actin polymerization (Fig. 2, *F* and *K*). Even after induction by MG132, a proteasome inhibitor, CLRN1$^{N48K}$ proteins did not induce F-actin-rich protrusions (supplemental Fig. S1*B*; a detailed characterization of CLRN1$^{N48K}$ will also be provided below). These results suggest that wild-type CLRN1 locally activates cellular spreading and an increase in the number of cellular protrusions.

*CLRN1 Forms a Membranous Microdomain*—The unique localization of CLRN1 at cellular protrusions suggests that it is enriched in specific parts of the plasma membrane. To determine whether CLRN1 is enriched in specific membrane compartments, we investigated the densities of clarin-1-enriched microdomains by using sucrose density gradient centrifugation, and compared them to the density of membrane microdomains containing the transferrin receptor (Fig. 3*A*), a membrane protein typically excluded from lipid rafts (27). When 0.5% Brij 98 was included in the membrane preparation, CLRN1 was detected in low density fractions, whereas most of the transferrin receptor was found in high density fractions. The low density of the clarin-1-enriched microdomains is reminiscent of lipid rafts that contain cholesterol. To determine

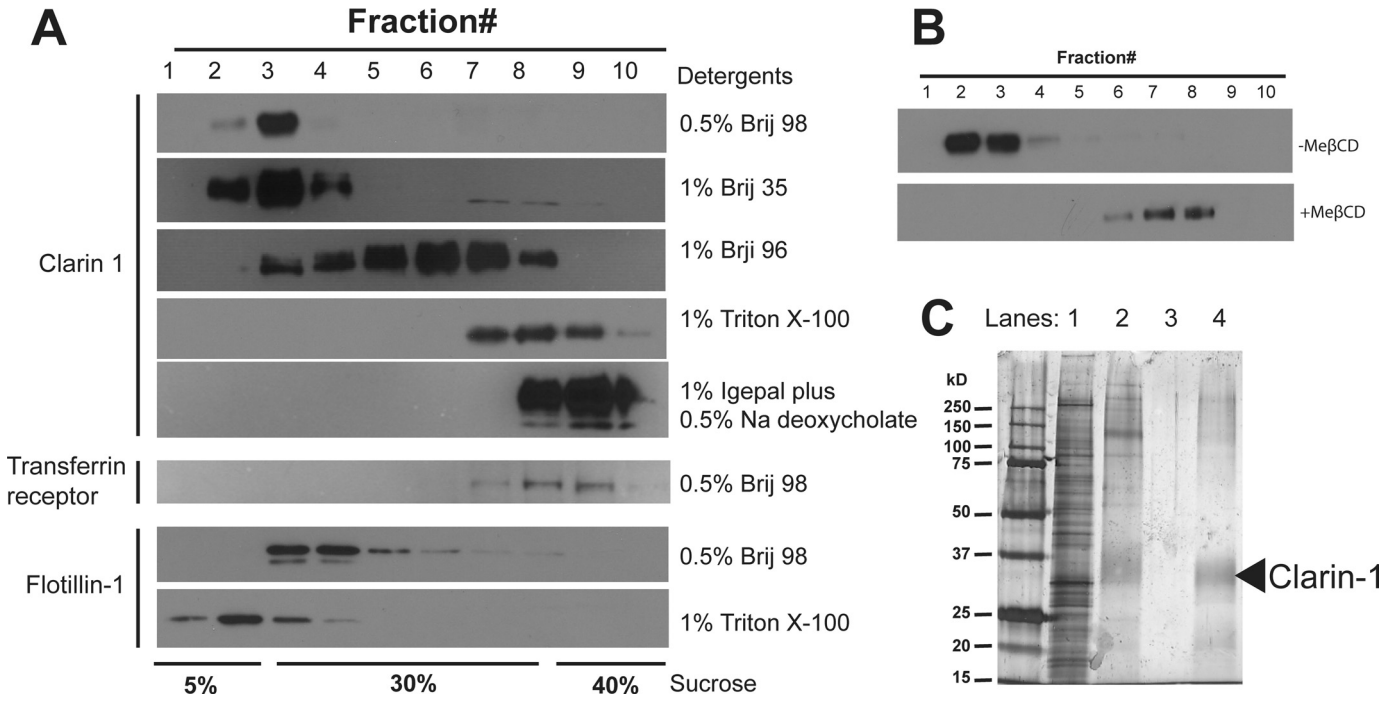


FIGURE 3. **Identification of clarin-1-enriched microdomains.** Human CLRN1 forms specific microdomains on plasma membranes. *A*, HEK-CLRN cells were lysed in buffer containing different detergents and analyzed in a discontinuous sucrose gradient. Ten fractions (0.4 ml) were collected from the *top* to the *bottom* of the gradient and analyzed by Western blotting for CLRN1 and transferrin receptor. Detergents shown on the *right* of the CLRN1 panel are listed from the *top* to *bottom* in order of increasing hydrophobicity. CLRN1 was enriched in low density fractions and shifted to higher density fractions with increasing detergent hydrophobicity. Localization of transferrin receptor, a transmembrane protein, was not affected by the hydrophobicity of detergents. Flotillin, a lipid raft protein, partitioned into low density fractions in the presence of either Triton X-100 or Brij-98. *B*, cholesterol depletion causes CLRN1 to move into higher density fractions. HEK-CLRN cells were treated without or with Me$\beta$CD for 30 min at 37 °C before being lysed in 0.5% Brij-98. The cell lysate was centrifuged in a discontinuous sucrose gradient, and CLRN1 was detected by Western blotting. Cholesterol depletion partially disrupted the membrane microdomains containing CLRN1. *C*, affinity purification of CLRN1 from crude membrane preparations of HEK-CLRN C1 cells. Proteins were resolved by 8% SDS-PAGE, and stained with silver nitrate. *Lane 1*, crude membrane preparation from HEK-CLRN-C1 cells; *lane 2*, CLRN1-protein complex purified from a crude membrane preparation of HEK-CLRN-C1 cells by HA affinity gel purification; *lane 3*, after blocking by HA epitope peptide, only a small amount of proteins from the crude membrane preparation bound to HA affinity gel; *lane 4*, In the presence of 1% Igpal and 0.5% sodium deoxycholate, CLRN1 was purified by the HA affinity gel. The location of purified CLRN1 is indicated by an *arrowhead*.

whether cholesterol contributes to the observed low density of CLRN1, we compared the density of clarin-1-enriched microdomains in the presence and absence of Me$\beta$CD, which binds and depletes membrane cholesterol. Clarin-1-enriched microdomains had higher densities in the presence of Me$\beta$CD than in its absence (Fig. 3*B*). Therefore, CLRN1 localizes to membrane compartments enriched with cholesterol.

To learn if hydrophobic interactions play a role in organizing clarin-1-enriched microdomains, we fractionated membranes in the presence of non-ionic detergents of increasing hydrophobicity (Fig. 3*A*, *top Clarin-1 panel*, compare Brij-35 to Triton X-100). Although clarin-1-enriched microdomains became denser in the presence of Brij-96 than in the presence of Brij-35, these resulting clarin-1 densities were still lower than those of the transferrin receptor-containing fractions separated in the presence of Brij-98 (Fig. 3*A*), the mildest detergent conditions used in this study. Only in the presence of Triton X-100 was the density of CLRN1-containing fractions indistinguishable from those high density fractions containing the transferrin receptor in the presence of Brij-98. These results indicate that hydrophobic interactions play a major role in the assembly of clarin-1-enriched microdomains. A remarkable difference was noted between clarin-1-enriched microdomains and lipid rafts. In the presence of Triton X-100, the lipid raft marker, flotillin, partitioned into low density fractions, in contrast to CLRN1 that partitioned into high density fractions. This observation agrees with the reported insolubility of lipid raft proteins in Triton X-100 (28) and indicates that clarin-1-enriched microdomains are distinct from lipid rafts.

*Identification of CLRN1 Interacting Proteins*—Anticipating that the function of clarin-1-enriched microdomains would primarily reflect their protein components, we found by antibody-affinity purification that CLRN1 purified together with several other proteins (Fig. 3*C*, *lane 2*). These CLRN1-protein interactions appeared to be specific, because CLRN1 (Fig. 3*C*, *arrowhead*) and CLRN1-interacting proteins were significantly enriched from the crude membrane preparation (Fig. 3*C*, compare *lanes 1* and *2*) and did not bind to the antibody-resin after it was blocked by epitope peptides (Fig. 3*C*, *lane 3*). These proteins also failed to bind to CLRN1 in the presence of 1% Igepal plus 0.5% sodium deoxycholate (Fig. 3*C*, *lane 4*), the detergent mixture that disrupted clarin-1-enriched microdomains (Fig. 3*A*). To obtain insight into the function of the CLRN1-interactome, we identified a number of CLRN1-interacting proteins by using liquid chromatography-mass spectrometry (Table 1). Most of these proteins are known to have transmembrane domains and exist on plasma membranes. Among them, members of the integrin, plasma membrane calcium-transporting ATPase, and junctional adhesion molecules appeared repeatedly (Table 1). The same protein families are known to interact

**TABLE 1**

**A list of proteins that specifically interact with CLRN1**

From a number of proteins found in our proteomics analysis, we considered the listed proteins to be significant interaction partners of Clarin-1, because they satisfied the following two criteria: 1) -fold change was higher than 4 (see also "Experimental Procedures"). The -fold change was calculated from the observed peak intensities of $^{16}$O- and $^{18}$O-peptides. 2) The locations in SDS-gel are consistent with their molecular weights.

| Protein name | Swiss-prot ID | Quantified peptides | -fold change |
|---|---|---|---|
| 4F2 cell-surface antigen heavy chain | P08195 | 6 | 4.9 |
| 78-kDa glucose-regulated protein | P11021 | 2 | 5.0 |
| ATP synthase subunit γ, mitochondrial | P36542 | 2 | 4.8 |
| Basigin | P35613 | 3 | >10 |
| N-cadherin | P19022 | 2 | >10 |
| Calnexin | P27824 | 8 | >10 |
| Carboxypeptidase D | O75976 | 11 | >10 |
| Catenin α-1 | P35221 | 5 | 4.1 |
| Cation-independent mannose-6-phosphate receptor | P11717 | 10 | >10 |
| CD166 antigen | Q13740 | 6 | >10 |
| CD276 antigen | Q5ZPR3 | 2 | >10 |
| Cell adhesion molecule 1 | Q9BY67 | 2 | >10 |
| Clarin-1 | P58418 | 3 | 5.4 |
| Coxsackievirus and adenovirus receptor | P78310 | 3 | >10 |
| Guanine nucleotide-binding protein G(i), α-2 subunit | P04899 | 4 | >10 |
| Guanine nucleotide-binding protein G(I)/G(S)/G(T) subunit beta-1 | P62873 | 5 | >10 |
| Heat shock 70-kDa protein 1 | P08107 | 3 | >10 |
| Integrin α-5 | P08648 | 2 | >10 |
| Integrin α-6 | P23229 | 1 | >10 |
| Integrin α-V | P06756 | 3 | 4.4 |
| Integrin β-1 | P05556 | 8 | >10 |
| Junctional adhesion molecule A | Q9Y624 | 2 | >10 |
| Junctional adhesion molecule C | Q9BX67 | 2 | >10 |
| Monocarboxylate transporter 1 | P53985 | 5 | >10 |
| Myelin protein zero-like protein 1 | O95297 | 5 | >10 |
| Myosin light polypeptide 6 | P60660 | 2 | 8.5 |
| Neuropilin-1 | O14786 | 2 | >10 |
| Neutral amino acid transporter B(0) | Q15758 | 2 | >10 |
| Plasma membrane calcium-transporting ATPase 1 | P20020 | 14 | 10.0 |
| Plasma membrane calcium-transporting ATPase 4 | P23634 | 2 | 4.1 |
| Prostaglandin F2 receptor negative regulator | Q9P2B2 | 6 | >10 |
| Protein 4.1 | P11171 | 2 | >10 |
| Ras-related C3 botulinum toxin substrate 1 | P63000 | 2 | 5.6 |
| Ras-related protein Rab-14 | P61106 | 4 | 5.3 |
| Ras-related protein Rab-9A | P51151 | 1 | 5.2 |
| Ras-related protein Ral-A | P11233 | 3 | >10 |
| Ras-related protein Rap-1A | P62834 | 3 | 8.2 |
| Secretory carrier-associated membrane protein 1 | O15126 | 5 | >10 |
| Secretory carrier-associated membrane protein 3 | O14828 | 4 | >10 |
| Sodium/potassium-transporting ATPase subunit α-1 | P05023 | 23 | 5.9 |
| Sodium/potassium-transporting ATPase subunit β-3 | P54709 | 4 | >10 |
| Solute carrier family 12 member 2 | P55011 | 2 | >10 |
| Syntaxin-12 | Q86Y82 | 3 | >10 |
| Syntaxin-4 | Q12846 | 2 | 7.6 |
| Syntaxin-6 | O43752 | 3 | >10 |
| Syntaxin-7 | O15400 | 5 | >10 |
| Transferrin receptor protein 1 | P02786 | 4 | >10 |
| Tumor-associated calcium signal transducer 1 | P16422 | 3 | >10 |
| Type-1 angiotensin II receptor-associated protein | Q6RW13 | 2 | >10 |
| Tyrosine-protein kinase-like 7 | Q13308 | 3 | 6.0 |
| Vesicle-associated membrane protein 3 | Q15836 | 2 | >10 |
| Voltage-dependent anion-selective channel protein 1 | P21796 | 3 | >10 |
| Voltage-dependent anion-selective channel protein 2 | P45880 | 3 | 5.2 |
| Zinc transporter ZIP14 | Q15043 | 2 | 4.5 |

indirectly with F-actin (29), consistent with our proposal that CLRN1 is involved in F-actin reorganization. Proteomics analysis, the procedure used to identify these interacting proteins, is a highly sensitive method, so special care must be taken to screen out "false positive" CLRN1-interacting proteins. False positive identification can occur by both specific and artificial binding of proteins to the affinity matrices (30). Accordingly, we took advantage of a proteolytic $^{18}$O-labeling technique to compare the amounts of each protein bound to the affinity beads that were either dependent or independent of the interaction with CLRN1. This comparative approach reliably distinguished the CLRN1 partners from other proteins interacting with the affinity beads.

To study the function of CLRN1 interactome in an unbiased way, we determined whether any molecular pathways were significantly enriched among the identified CLRN1-associated proteins by using the Gene Set Analysis Toolkit (31). Significant enrichment was observed in protein components of pathways related to cell adhesion/migration, focal adhesion, tight junctions, and actin cytoskeleton regulation (supplemental Fig. S2, $p \leq 0.0000163$ calculated from a hypergeometric test using the human genome as a reference). The specific functions of identified proteins and pathways affirm that the function of the CLRN1-interactome is related to the organization of membrane structures supported by the actin cytoskeleton.

*CLRN1 Facilitates Assembly of Its Interactive Partners at Lamellipodia*—Among all the identified membrane proteins, integrins and N-cadherin play essential roles in cell motility. Integrin heterodimers activate cell motility by contributing to the formation of cell matrix contacts. Consistent with the inter-

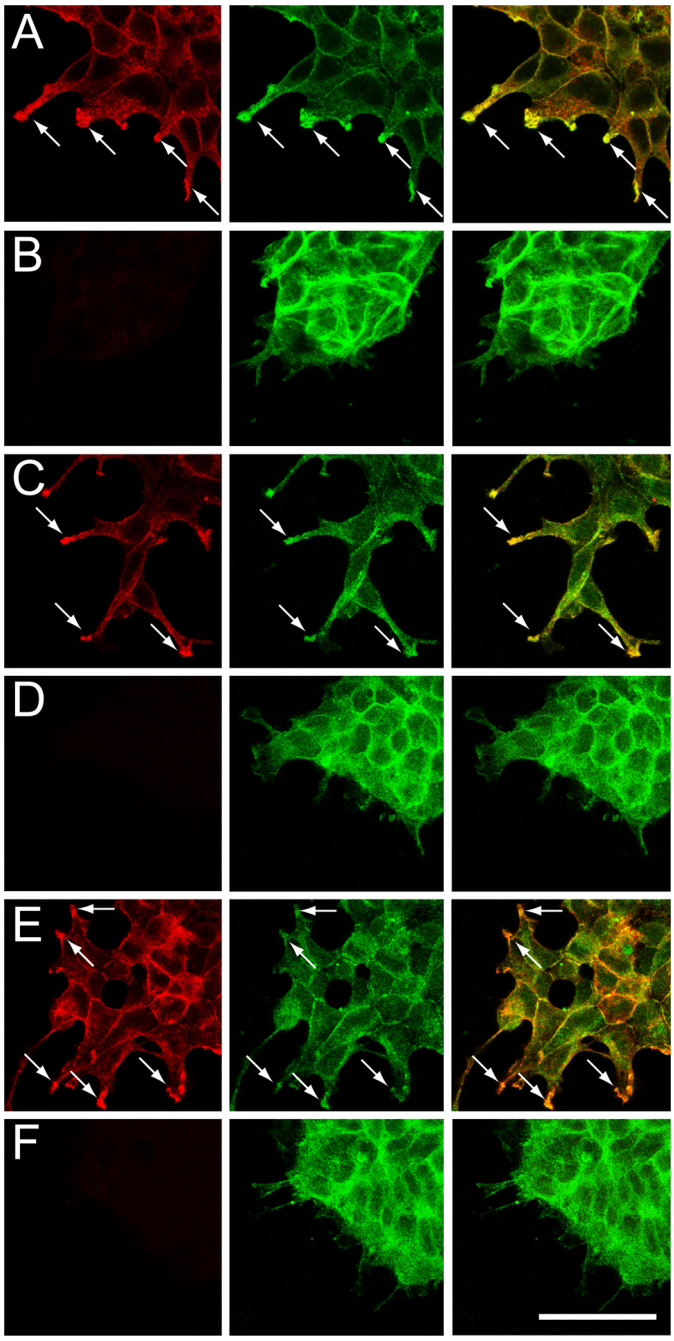


FIGURE 4. **CLRN1 induces compartmentalization of integrin, N-cadherin, and α-catenin.** HEK-CLRN C1 cells were co-stained with 10B5-Cy3 (mAb anti-CLRN1, *red*, images in the *left column*) and one of following mAbs (*green*, images in the *middle column*): anti-integrin-β1 subunit (*A*), anti-N-cadherin (*C*), and anti-α-catenin (*E*). *Arrows* indicate some locations where CLRN1 and integrin/N-cadherin/α-catinin co-localize (*yellow* or *orange*, images in the *right column*). HEK293 cells were co-stained with 10B5-Cy3 (mAb anti-CLRN1, *red*, images in the *left column*) and one of the following mAbs (*green*, images in the *middle column*): anti-integrin-β1 subunit (*B*), anti-N-cadherin (*D*), or anti-α-catenin (*F*). The distribution of integrin, N-cadherin, or α-catinin is more uniform on the plasma membrane in the absence (*B*, *D*, and *F*) than in the presence (*A*, *C*, and *E*) of CLRN1. Images are single optical sections. *Scale bar*, 50 μm.

action of CLRN1 with integrin, confocal microscopy revealed their co-localization at cellular protrusions (Fig. 4*A*). Integrin was less prone to accumulate at the cellular protrusions in the absence of CLRN1, but instead, localized uniformly on the plasma membrane of HEK293 cells (Fig. 4*B*).

In contrast to integrin, N-cadherin plays an important role in cell-cell adhesion through its homophilic interactions, and furthermore, it can promote the motility of cancer cells, possibly through the fibroblast growth factor receptor signaling pathway (32). Consistent with N-cadherin interactions with CLRN1, N-cadherin was attracted to the cellular protrusions of the HEK-CLRN C1 cell line (Fig. 4*C*). In HEK293 cells that did not express CLRN1, N-cadherin was barely detectable at the lamellipodia but was highly concentrated at cell-cell contacts (Fig. 4*D*). Similar localization patterns were observed for another CLRN1-interacting protein α-catenin (Fig. 4, *E* and *F*), which also interacts with N-cadherin. These studies suggest that CLRN1 promotes assembly of its interacting partners at cellular protrusions. Feasibly CLRN1 could activate cell motility via N-cadherins, either through the fibroblast growth factor receptor signaling pathway or by attenuating their homophilic interactions. Consistent with the latter idea, N-cadherin and α-catenin immunofluorescence was more intense at cell-cell contacts of HEK293 cells than those of HEK-CLRN stable cells.

*CLRN1 Requires N-Linked Glycosylation for Folding and Localization to the Plasma Membrane*—From its primary structure, CLRN1 is predicted to be an *N*-linked glycoprotein (Fig. 1*A*). *N*-Linked glycosylation is often used for recognition by the chaperone proteins, calnexin and calreticulin. When expressed in HEK293 cells, most of CLRN1 was *N*-glycosylated, as shown by the major isoforms exhibiting molecular masses between 26 and 37 kDa (Fig. 5*A*, *lane 1*, **). The *N*-linked glycosylation was ablated by treatment with PNGase F (Fig. 5*A*, *lane 2*, *) but was resistant to Endo $H_f$ (Fig. 5*A*, *lane 3*). Resistance to Endo $H_f$ suggests that the *N*-linked glycan moiety on CLRN1 was processed by Golgi-mannosidase II and passed through the protein quality control mechanism of the Golgi apparatus. Therefore, the observed glycosylation pattern is also consistent with the localization of CLRN1 to the plasma membrane (Fig. 1).

The point mutation that replaces asparagine at position 48 with lysine was found to be the major cause of Usher syndrome III in North America (4, 5). To study the function of *N*-linked glycosylation in CLRN1, we established stable HEK 293 cells that expressed $CLRN1^{N48K}$ (HEK-$CLRN^{N48K}$). We also were able to amplify $CLRN1^{N48K}$ cDNA, suggesting active transcription of the $CLRN1^{N48K}$ transgene from HEK-$CLRN^{N48K}$ cells (supplemental Fig. S1), but immunofluorescence from $CLRN1^{N48K}$ was barely detectable in HEK-$CLRN^{N48K}$ cells (Fig. 5*B*, *top row*). *N*-Linked glycosylation is often required for proper folding of membrane proteins, and we consistently observed the interaction of wild-type CLRN1 with calnexin, a glycoprotein-specific chaperone (Table 1). We therefore investigated whether poor expression of $CLRN1^{N48K}$ was due to the degradation of misfolded $CLRN1^{N48K}$. Consistent with the degradation of N48K clarin-1 by the ubiquitin-proteasome pathway, the expression level of $CLRN1^{N48K}$ was increased by treatment of HEK-$CLRN^{N48K}$ cells with the proteasome inhibitor MG132 (Fig. 5, *A* and *B*). $CLRN1^{N48K}$ expressed in HEK293 cells showed molecular masses indistinguishable from CLRN1 deglycosylated by PNGase F (Fig. 5*A*, *lanes 2* and *4*) and were unchanged by either PNGase F or Endo H treatment (Fig. 5*A*,

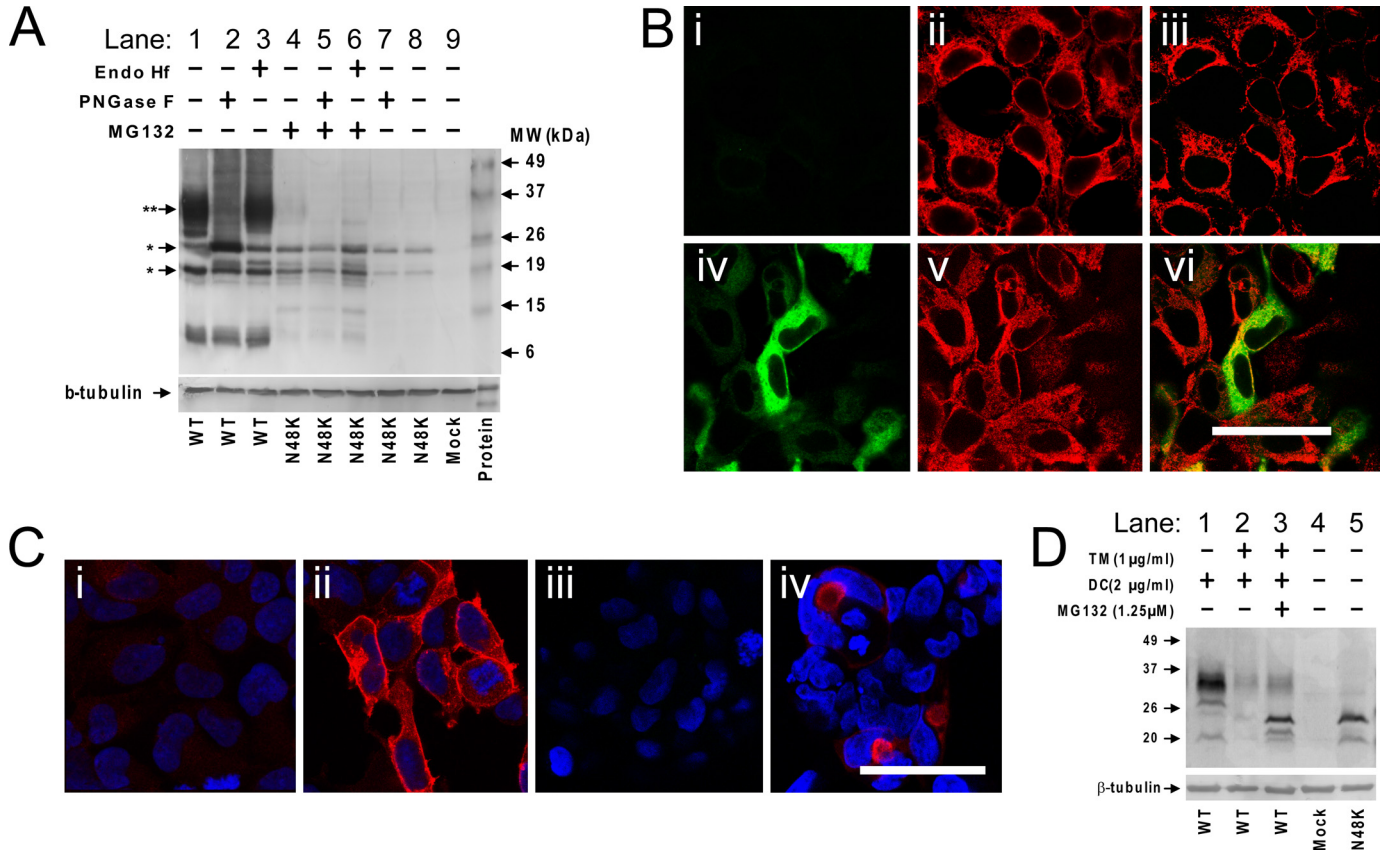


FIGURE 5. ***N*-Linked glycosylation is required for the stability and plasma membrane localization of CLRN1.** *A*, Western blotting analysis of HEK293 cells stably expressing human CLRN1 and CLRN1$^{N48K}$ (*top gel image*). Five samples were treated with either Endo $H_f$ or PNGase F to study glycosylation patterns. Three samples were treated with MG132 to inhibit degradation of CLRN1$^{N48K}$ by proteasomes. Combinations of those treatments are indicated above the *top gel image*. **, position corresponding to glycosylated wild-type CLRN1; *, position of non-glycosylated CLRN1. The cell type used for each sample is shown below the *bottom gel image*; *WT* represents stable cells expressing wild-type human CLRN1, N48K represents stable cells expressing CLRN1$^{N48K}$, and MOCK represents HEK 293 cells. Anti-$\beta$-tubulin antibody was used to study the loading of each sample (*bottom gel image*). *B*, localization of human CLRN1$^{N48K}$ mutant in HEK293 cells. *Top row*: *i*, expression of CLRN1$^{N48K}$ (*green* immunofluorescence) is barely detectable under normal conditions; *ii*, cells were stained with anti-calreticulin (*red*), a marker for the endoplasmic reticulum; *iii*, *merged image* of *i* and *ii*. *Bottom row*: *iv*, after MG132 treatment, expression of CLRN1$^{N48K}$ is detectable as shown by *green* immunofluorescence; *v*, cells were stained with anti-calreticulin; *vi*, *merged image* of *iv* and *v*. CLRN1$^{N48K}$ localized to the endoplasmic reticulum, as shown by co-localization of calreticulin and CLRN1$^{N48K}$; CLRN1$^{N48K}$ is also observed in the cytoplasm. *C*, tunicamycin promotes proteasome-mediated degradation of wild-type CLRN1. In this experiment, CLRN1 expression was regulated by a doxycycline-inducible promoter in HEK293-CLRN-ind cells. *i*, in the absence of doxycycline, CLRN1 was not detected; *ii*, 24 h after doxycycline induction, most of the CLRN1 (*red*) was observed on plasma membranes; *iii*, combination treatment with doxycycline and tunicamycin abolished the expression of CLRN1; *iv*, after treatment of the cells with doxycycline, tunicamycin, and MG132, CLRN1 (*red*) was noted as intracellular inclusions. Nuclei were stained with Hoechst 33342 (*blue*). *D*, Western blotting analysis of HEK293-CLRN-ind cells. Two samples were treated with tunicamycin (*TM*) to inhibit *N*-linked glycosylation, and three samples were treated with doxycycline (*DC*) to induce expression of CLRN1. Cells used for *lane 3* were also treated with MG132. Combinations of these treatments are indicated over the *gel images*. The cell type used for each *lane* is indicated below the *gel images*: WT are from HEK-CLRN-ind, N48K are from HEK-CLRN$^{N48K}$, and MOCK are from HEK 293 cells. $\beta$-Tubulin antibody was used to study the loading of each sample (*bottom gel images*). *Images* in *B* and *C* are single optical sections. *Scale bar*, 50 $\mu$m.

*lanes 5* and *6*). These results indicate that the asparagine at position 48 is the only *N*-linked glycosylation site of CLRN1, and they experimentally confirm that the first extracellular loop of CLRN1 faces the extracellular side.

The above experiments indicate that N48K mutant proteins are degraded by proteasomes and are not glycosylated. The question still remains as to whether the mutant proteins are misfolded either because of the lack of glycosylation or a structural abnormality resulting from the replacement of asparagine with lysine at position 48. To differentiate between those two possibilities, we determined how lack of glycosylation, conferred by pretreatment with tunicamycin (33, 34), influences the folding of wild-type CLRN1. Stable HEK293 cells were generated in which the expression of CLRN1 was triggered by doxycycline, and such treatment of these cells induced the expression of wild-type CLRN1 (Fig. 5, *C* and *D*). After induction, wild-type CLRN1 localized mainly to the plasma membrane (Fig. 5*C*, *i* and *ii*). Then we treated these cells with both doxycycline and tunicamycin to cause deficient *N*-linked glycosylation of newly synthesized wild-type CLRN1. The expression level of CLRN1 was lower in cells treated with both tunicamycin and doxycycline than with doxycycline alone (Fig. 5*C*, *ii* and *iii*, also see Fig. 5*D*, *lanes 1* and *2*). To confirm that wild-type CLRN1 is synthesized under tunicamycin treatment but degraded by proteasomes, we treated these cells with the proteasome inhibitor MG-132, in addition to tunicamycin and doxycycline. MG132 treatment increased the expression level of wild-type CLRN1 in cellular inclusions (Fig. 5, *C* (*iv*) and *D* (*lanes 2* and *3*)), indicating that CLRN1 is translated in the presence of tunicamycin. These observations suggest that a cellular deficiency in *N*-linked glycosylation leads to degradation of wild-type CLRN1 by a mechanism similar to the degradation

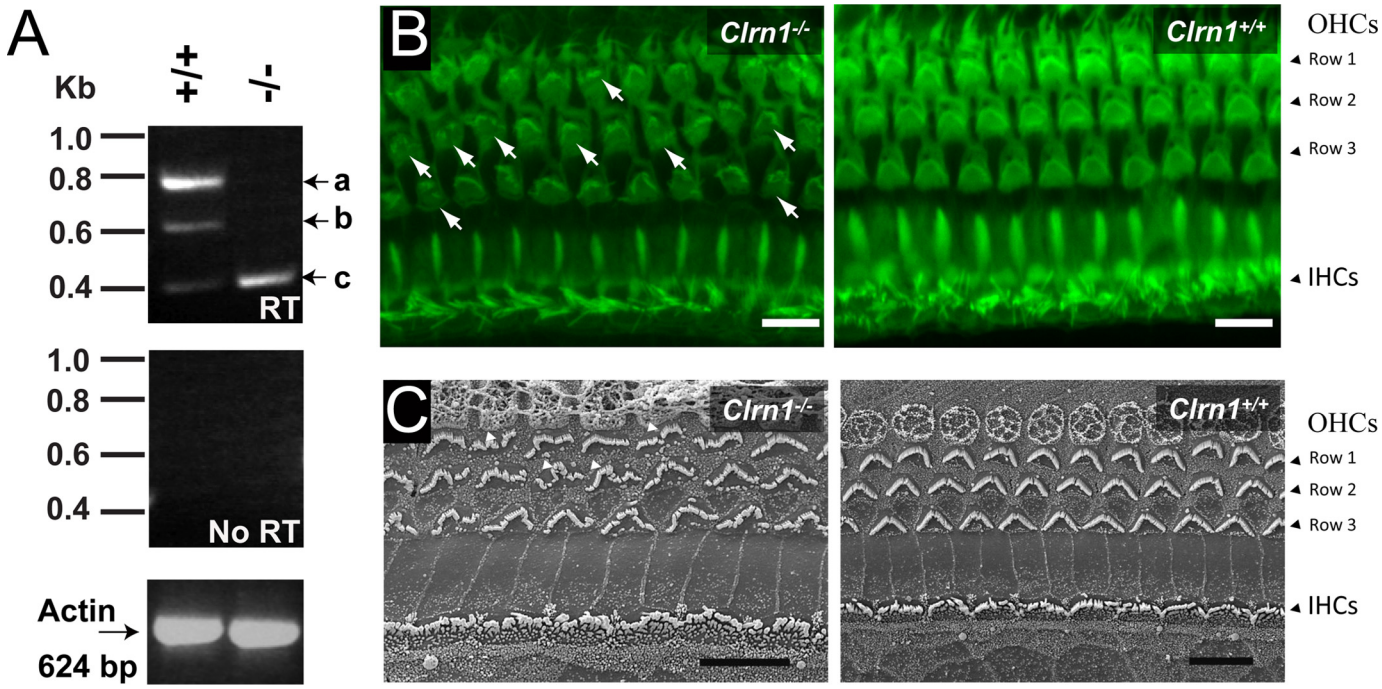


FIGURE 6. **F-actin-enriched stereocilia are poorly developed in cochlear hair cells of *Clrn1* knock-out mice.** *A*, *Clrn1* knock-out (*Clrn1*$^{-/-}$) mice did not express full-length *Clrn1* mRNA in the cochlea (*RT panel*). Total RNA was isolated from the cochlea and used for RT-PCR. Total RNA without reverse transcription reaction (*no RT panel*) was used as a negative control to confirm that cDNAs, instead of genomic DNAs, were amplified by PCR. As an internal control, actin cDNA was amplified to confirm that a similar amount of mRNA was used for each experiment. Based on sequencing analysis, *band a* was composed of two splicing variants: one with all four exons and the other with exons 1, 3, and 4. *Band b* was a transcript with exons 1 and 4. *Band c* was a nonspecific product. *B*, organs of Corti from *Clrn1*$^{-/-}$ (*left panel*) and *Clrn1*$^{+/+}$ (*right panel*) mice were fluorescently labeled with Alexa 488-labeled phalloidin to reveal F-actin structures in *green*. F-actin-enriched stereocilia were poorly developed in *Clrn1*$^{-/-}$ outer hair cells, whereas V-shaped bundles of stereocilia were observed in *Clrn1*$^{+/+}$ outer hair cells. Images were generated from multiple optical sections by a maximum intensity projection. In *C*: *left panel*, *Clrn1*$^{-/-}$ mice show disorganization of OHC stereocilia (*white arrowheads*) and the inner hair cells (*IHCs*) evidence subtle changes in stereocilial organization. *Right panel*, wild-type mouse illustrating normally configured V-shaped stereocilia in outer hair cells (*OHCs*, *rows 1–3*) and crescent-shaped bundles in IHCs. *Scale bars*, 10 $\mu$m.

of CLRN1$^{N48K}$. Collectively, our data indicate that lack of glycosylation in N48K mutants leads to misfolding, mislocalization, and degradation of the protein. With proper glycosylation (Fig. 5*D*, *lane 1*), wild-type CLRN1 is transported to the plasma membrane, where it can exert its cellular function.

*CLRN1 Is Essential for the Structural Integrity and Arrangement of Stereocilia in Auditory Hair Cells*—If CLRN-1 is essential for F-actin organization, then F-actin-enriched organelles such as stereocilia should show structural abnormalities in the *Clrn1* knock-out (*Clrn1*$^{-/-}$) mouse[4] (Fig. 6*A*). To test this hypothesis, we analyzed the stereocilia organization in auditory hair cells by confocal and scanning electron microscopy. By confocal microscopy of Alexa 488-labeled organs of Corti, *Clrn1*$^{-/-}$ mice showed disorganization of F-actin-enriched stereocilia at the age of postnatal day 18 (Fig. 6*B*, *left*). Outer hair cells failed to reveal symmetrically V-shaped stereocilia, and the stereocilia appeared fewer in number (Fig. 6*B*, *left*, *arrows*) compared with hair cells from the *Clrn1*$^{+/+}$ specimen (Fig. 6*B*, *right*). As expected, all the examined *Clrn1*$^{+/+}$ outer hair cells showed regularly V-shaped stereocilia (Fig. 6*B*, *right*). At postnatal day 10, stereocilia disorganization was already detectable by scanning electron microscopy (Fig. 6*C*, *left*); *Clrn1*$^{-/-}$ mice exhibited disorganized stereocilia, as contrasted to *Clrn1*$^{+/+}$ mice with uniformly arranged stereocilia (Fig. 6*C*). These structural abnormalities were more obvious in outer than in inner hair cells. Although the structures were abnormal in *Clrn1*$^{-/-}$ mice, the hair cells still maintained their planar cell polarity at this stage; the tip of distorted "V" bundles of outer hair cells were pointing toward the lateral edge of the cochlea, and there was no evidence that the stereocilia of the inner hair cells lack polarity either. Therefore, CLRN1 is not involved in the establishment of planar cell polarity. Instead, the phenotype of the auditory hair cells of *Clrn1*$^{-/-}$ mice is consistent with the proposed role of CLRN1 in the maintenance and organization of F-actin-enriched organelles.

## DISCUSSION

Here we report formation of a novel plasma membrane subdomain; the clarin-1-enriched microdomain, in HEK293 cells. Clarin-1-enriched microdomains contain specific proteins functioning in cell-adhesion/migration and regulation of the actin cytoskeleton. Evidence is provided that the possible function of clarin-1-enriched microdomains is the local activation of actin polymerization. CLRN1 localized to sites of actin polymerization, and induced the mobility of HEK293 cell by increasing the number of lamellipodia. In contrast, the CLRN1$^{N48K}$ functionally null mutant did not induce these phenotypic changes in HEK293 cells, and the lack of glycosylation associated with the CLRN1$^{N48K}$ mutant led instead to mislocalization and degradation of CLRN1$^{N48K}$. Consistent with a previous study on the pathology associated with the N48K *CLRN1*

[4] A detailed characterization of hearing phenotype in *Clrn1*$^{-/-}$ mouse has been published recently (56).

mutation in patients (16), our results indicate that proper function of CLRN1 requires its localization to the sub-plasma membrane compartment. Further supporting the indirect interaction of clarin-1-enriched microdomains and actin, a number of the CLRN1-interacting proteins (see Table 1) are known to regulate the organization of actin filaments. For example, $\alpha$-catenin binds to actin filaments via vinculin and $\alpha$-actinin (35), and junctional adhesion molecules A and C bind to actin through their interaction with ZO-1 (36). Integrins incorporate a number of proteins that regulate actin filaments. Downstream in the integrin signaling pathway, the small G-protein Rac1 (Ras-related C3 botulinum toxin substrate 1 in Table 1) is capable of activating lamellipodia formation (37). The integrin $\beta$1 subunit, found to interact with CLRN1, is one of the integrin components required for regulation of F-actin in stereocilia of utricular hair cells in the inner ear (38). Another CLRN1-interacting protein, neuropilin, acts upstream in the pathway for axon guidance that also involves the reorganization of actin filaments. Therefore, morphological changes of HEK293 cells induced by CLRN1 can be explained by a multitude of partner proteins related to cell-adhesion/migration and regulation of the actin cytoskeleton at lamellipodial protrusions.

Clarin-1-enriched microdomains and tetraspanin-enriched microdomains exhibit properties distinct from other plasma membrane microdomains such as lipid rafts, caveolae, or glycosylphosphatidylinositol-anchored proteins (domain). Unlike lipid rafts, clarin-1-enriched microdomains (this study), and tetraspanin-enriched-microdomains (39, 40) are only partially disrupted by cholesterol depletion and completely disrupted by Triton X-100 treatment. From our proteomics study (Table 1), Clarin-1-enriched microdomains were significantly enriched with some components of tetraspanin-enriched microdomains, such as integrins, syntaxin-4, and Prostaglandin F2 receptor negative regulator (CD9P-1) (41–43). Clarin-1-enriched microdomains, however, were not enriched with the markers of lipid rafts and caveolae, such as flotillin 1, lyn tyrosine kinase, SNAP-23, or caveolin (44–46). Furthermore, we failed to discover significant interactions of Clarin-1 with glycosylphosphatidylinositol-anchored proteins that were predicted by big-PI Predictor (available on the Web). One unexpected finding was that the transferrin receptor interacted with CLRN1 (Table 1), even though most of the CLRN1 and transferrin receptor partitioned into membrane fractions with different densities (Fig. 3). This apparently contradictory observation could be explained either by a high affinity interaction of CLRN1 with transferrin receptors that exists at low concentrations in low density fractions, or by interactions at the interface between two lipid plasma membrane domains. This unusual interaction of CLRN1 and transferrin also distinguishes clarin-1-enriched microdomains from regular lipid rafts that typically do not associate with transferrin receptors.

Although CLRN1 microdomains are similar to tetraspanin-enriched microdomains, structural differences between the two were noted. Unlike tetraspanin, CLRN1 does not conserve the structurally essential cysteine residues in the second extracellular loop that tetraspanins dedicate to forming intramolecular disulfide-bonds. These disulfide bonds were found to be required for the heterophilic interaction of tetraspanin with its cognate integrin, as well as for the homophilic interaction between tetraspanins themselves (47). Although CLRN1 has no cysteine residues in the second extracellular loop, significant interactions between CLRN1 and integrin subunits still occur. Therefore, the structural determinants for CLRN1-integrin interactions differ from those involved in tetraspanin-integrin interactions. Other important cysteine residues of tetraspanins are dedicated to *S*-palmitoylation, which is important for heterophilic interactions among tetraspanins (48–50). Unlike tetraspanins, the structure of CLRN1 does not predict a membrane-juxtaposed *S*-palmitoylation site. Possibly the absence of such palmitoylation is the reason why we failed to document a heterophilic interaction of CLRN1 with the tetraspanins. There are some CLRN1-interactive partners that were not seen in tetraspanin-enriched microdomains. Those unique components include cell adhesion molecule 1, protein 4.1, neuropilin-1, and junctional adhesion molecule A/C. To our knowledge, this unique combination of proteins has not been found in other membrane microdomains. As exemplified by the differences in the cysteine residues and the interactive partners, we predict that molecular interactions involved in clarin-1-enriched microdomains differ significantly from tetraspanin-enriched microdomains.

Our studies also provide additional insights into molecular relationships between CLRN1 and Usher type I and II gene products. CLRN1 regulates the actin cytoskeleton, known to be a critical core of the Usher syndrome-interaction network. Consistent with *in vitro* studies, *Clrn1*$^{-/-}$ mice showed disorganized stereocilial structures in inner and outer hair cells, where the Usher-interaction network operates. One of the links between CLRN1/actin and Usher type I products is the direct interaction of myosin VIIa with actin filaments (51, 52). Previously, a genetic interaction between Usher syndrome types IB and IIIA was reported in which the single null allele of type 1B increased the severity of deafness in patients with two null type IIIA alleles. This genetic interaction is consistent with a possible indirect interaction between the corresponding gene products, CLRN1 and myosin VIIa, as suggested in this study. Another possible link between CLRN1 and Usher type I is the harmonin-actin interaction. Harmonin directly interacts with F-actin and induces F-actin resistance to depolymerizing agents such as cytochalasin D (10). Our studies indicate that harmonin and CLRN1 work at different steps to increase the amount of F-actin. Unlike the interaction of harmonin-b with actin, the CLRN1-actin interaction is weak and possibly indirect, because CLRN1 does not induce F-actin resistance to cytochalasin D. Another piece of evidence for an indirect interaction of CLRN1 with actin is that binding of CLRN1 to actin was readily disrupted by 0.5% Brij-98 (supplemental Fig. S3), even though the clarin-1-enriched microdomain was stable under identical conditions (Fig. 3). Therefore, in the Usher protein network, our studies suggest that CLRN1 increases the amount of F-actin filaments at a step distinct from harmonin. A link between CLRN1 and Usher II gene products can be established through the interaction of CLRN1 with protein 4.1. Protein 4.1 binds indirectly to whirlin, an Usher type IID protein,

along with the membrane-associated MAGUS family protein, p55 (53). Our studies support and extend the previously proposed hypothesis that Usher proteins interact together to form an intricate network wherein deficiencies can lead to similar disease phenotypes of variable severity (reviewed in Refs. 2, 9). CLRN1 is expressed both in the inner and outer hair cells, where Usher type I–III interactions occur. Inside the network, harmonin and whirlin act as adaptors between CLRN1 and other Usher gene products, through their multiple PDZ domains.

In summary, this study provides an initial step in understanding CLRN1 function at the cellular level, namely that this protein is critical to the organization of components that possibly regulate the actin cytoskeleton. Among the protein components of Clarin-1-enriched microdomains, proteins directly interacting with CLRN1 remain to be established. Identification of such direct interacting partners will lead to more precise understanding of CLRN1 function in regulating the actin cytoskeleton. Defects in gene products that regulate F-actin organization lead to inner ear and retinal disorders, and therefore, it would be intriguing to learn whether CLRN1 and other actin regulators of the eye and ear are in the same signaling network. The regulatory function of CLRN1 is unique among the diverse Usher gene products. It is difficult to understand why pleiotropic diseases such as Bardet-Biedl syndrome and Usher syndrome share similar pathologies despite mutations in a functionally diverse group of genes. The recent discovery of the BBSome, a stable protein complex composed of Bardet-Biedl syndrome gene products (54), may unify roles of these diverse gene products into a single pathological pathway. By analogy, possible interactions of Usher type I, II, and III genes suggested by this and other studies should shed light on a common pathological pathway for the Usher syndrome.

*Acknowledgments—We appreciate the vision, inspiration, and generosity of the Elden family that made this work possible. We are grateful to Dr. Charles G. Wright (Dept. of Otolaryngology, Southwestern Medical Center) for his assistance on the electron microscopy analysis of the mouse cochlea. We also thank Chie Iioka for her technical assistance in culturing cells and establishing cell lines. The monoclonal antibodies developed by Drs. M. Klymkowsky and D. M. Fambrough were obtained from the Developmental Studies Hybridoma Bank developed under the auspices of the NICHD and maintained by The University of Iowa, Dept. of Biological Sciences, Iowa City, Iowa. We thank Dr. Emhonta Johnson (Dept. of Pharmacology, Case Western Reserve University) for providing us with anti-N-cadherin (13A9) and anti-α-catenin (1G5). We thank Dr. Leslie T. Webster, Jr. for valuable comments on the manuscript.*

## REFERENCES


1. Saihan, Z., Webster, A. R., Luxon, L., and Bitner-Glindzicz, M. (2009) *Curr. Opin. Neurol.* **22,** 19–27
2. Reiners, J., Nagel-Wolfrum, K., Jürgens, K., Märker, T., and Wolfrum, U. (2006) *Exp. Eye Res.* **83,** 97–119
3. Williams, D. S. (2008) *Vision Res.* **48,** 433–441
4. Adato, A., Vreugde, S., Joensuu, T., Avidan, N., Hamalainen, R., Belenkiy, O., Olender, T., Bonne-Tamir, B., Ben-Asher, E., Espinos, C., Millán, J. M., Lehesjoki, A. E., Flannery, J. G., Avraham, K. B., Pietrokovski, S., Sankila, E. M., Beckmann, J. S., and Lancet, D. (2002) *Eur. J. Hum. Genet.* **10,** 339–350
5. Fields, R. R., Zhou, G., Huang, D., Davis, J. R., Möller, C., Jacobson, S. G., Kimberling, W. J., and Sumegi, J. (2002) *Am. J. Hum. Genet.* **71,** 607–617
6. Joensuu, T., Hämäläinen, R., Yuan, B., Johnson, C., Tegelberg, S., Gasparini, P., Zelante, L., Pirvola, U., Pakarinen, L., Lehesjoki, A. E., de la Chapelle, A., and Sankila, E. M. (2001) *Am. J. Hum. Genet.* **69,** 673–684
7. Maecker, H. T., Todd, S. C., and Levy, S. (1997) *FASEB J.* **11,** 428–442
8. Hemler, M. E. (2005) *Nat. Rev. Mol. Cell Biol.* **6,** 801–811
9. Kremer, H., van Wijk, E., Märker, T., Wolfrum, U., and Roepman, R. (2006) *Hum. Mol. Genet.* **15,** R262–R270, review
10. Boëda, B., El-Amraoui, A., Bahloul, A., Goodyear, R., Daviet, L., Blanchard, S., Perfettini, I., Fath, K. R., Shorte, S., Reiners, J., Houdusse, A., Legrain, P., Wolfrum, U., Richardson, G., and Petit, C. (2002) *EMBO J.* **21,** 6689–6699
11. McGee, J., Goodyear, R. J., McMillan, D. R., Stauffer, E. A., Holt, J. R., Locke, K. G., Birch, D. G., Legan, P. K., White, P. C., Walsh, E. J., and Richardson, G. P. (2006) *J. Neurosci.* **26,** 6543–6553
12. Michalski, N., Michel, V., Bahloul, A., Lefèvre, G., Barral, J., Yagi, H., Chardenoux, S., Weil, D., Martin, P., Hardelin, J. P., Sato, M., and Petit, C. (2007) *J. Neurosci.* **27,** 6478–6488
13. Mogensen, M. M., Rzadzinska, A., and Steel, K. P. (2007) *Cell Motil. Cytoskeleton* **64,** 496–508
14. Lefèvre, G., Michel, V., Weil, D., Lepelletier, L., Bizard, E., Wolfrum, U., Hardelin, J. P., and Petit, C. (2008) *Development* **135,** 1427–1437
15. Adato, A., Kalinski, H., Weil, D., Chaib, H., Korostishevsky, M., and Bonne-Tamir, B. (1999) *Am. J. Hum. Genet.* **65,** 261–265
16. Herrera, W., Aleman, T. S., Cideciyan, A. V., Roman, A. J., Banin, E., Ben-Yosef, T., Gardner, L. M., Sumaroka, A., Windsor, E. A., Schwartz, S. B., Stone, E. M., Liu, X. Z., Kimberling, W. J., and Jacobson, S. G. (2008) *Invest. Ophthalmol. Vis. Sci.* **49,** 2651–2660
17. Maeda, M., Johnson, E., Mandal, S. H., Lawson, K. R., Keim, S. A., Svoboda, R. A., Caplan, S., Wahl, J. K., 3rd, Wheelock, M. J., and Johnson, K. R. (2006) *Oncogene* **25,** 4595–4604
18. Johnson, E., Theisen, C. S., Johnson, K. R., and Wheelock, M. J. (2004) *J. Biol. Chem.* **279,** 31041–31049
19. Tian, G., Lai, L., Guo, H., Lin, Y., Butchbach, M. E., Chang, Y., and Lin, C. L. (2007) *J. Biol. Chem.* **282,** 1727–1737
20. Butchbach, M. E., Tian, G., Guo, H., and Lin, C. L. (2004) *J. Biol. Chem.* **279,** 34388–34396
21. Kikkawa, Y. S., Pawlowski, K. S., Wright, C. G., and Alagramam, K. N. (2008) *Anat. Rec.* **291,** 224–232
22. Yuan, C., Sheng, Q., Tang, H., Li, Y., Zeng, R., and Solaro, R. J. (2008) *Am. J. Physiol. Heart Circ. Physiol.* **295,** H647–656
23. Kiser, J., Post, M., Wang, B., and Miyagi, M. (2009) *J. Proteome Res.* **8,** 1810–1817
24. Miyagi, M., and Rao, K. C. (2007) *Mass Spectrom. Rev.* **26,** 121–136
25. Pawlowski, K. S., Kikkawa, Y. S., Wright, C. G., and Alagramam, K. N. (2006) *J. Assoc. Res. Otolaryngol.* **7,** 83–94
26. Rizzolo, L. J., and Zhou, S. (1995) *J. Cell Sci.* **108,** 3623–3633
27. Harder, T., Scheiffele, P., Verkade, P., and Simons, K. (1998) *J. Cell Biol.* **141,** 929–942
28. Simons, K., and Toomre, D. (2000) *Nat. Rev. Mol. Cell Biol.* **1,** 31–39
29. Fujimoto, T. (1993) *J. Cell Biol.* **120,** 1147–1157
30. Trinkle-Mulcahy, L., Boulon, S., Lam, Y. W., Urcia, R., Boisvert, F. M., Vandermoere, F., Morrice, N. A., Swift, S., Rothbauer, U., Leonhardt, H., and Lamond, A. (2008) *J. Cell Biol.* **183,** 223–239
31. Zhang, B., Schmoyer, D., Kirov, S., and Snoddy, J. (2004) *BMC Bioinformatics* **5,** 16
32. Nieman, M. T., Prudoff, R. S., Johnson, K. R., and Wheelock, M. J. (1999) *J. Cell Biol.* **147,** 631–644
33. Takatsuki, A., and Tamura, G. (1971) *J. Antibiot.* (*Tokyo*) **24,** 785–794
34. Duksin, D., and Bornstein, P. (1977) *J. Biol. Chem.* **252,** 955–962
35. Kobielak, A., and Fuchs, E. (2004) *Nat. Rev. Mol. Cell Biol.* **5,** 614–625
36. Itoh, M., Nagafuchi, A., Moroi, S., and Tsukita, S. (1997) *J. Cell Biol.* **138,** 181–192

37. Nobes, C. D., and Hall, A. (1995) *Cell* **81,** 53–62
38. Littlewood Evans, A., and Müller, U. (2000) *Nat. Genet.* **24,** 424–428
39. Israels, S. J., and McMillan-Ward, E. M. (2007) *Thromb. Haemost.* **98,** 1081–1087
40. Claas, C., Stipp, C. S., and Hemler, M. E. (2001) *J. Biol. Chem.* **276,** 7974–7984
41. Le Naour, F., André, M., Boucheix, C., and Rubinstein, E. (2006) *Proteomics* **6,** 6447–6454
42. André, M., Le Caer, J. P., Greco, C., Planchon, S., El Nemer, W., Boucheix, C., Rubinstein, E., Chamot-Rooke, J., and Le Naour, F. (2006) *Proteomics* **6,** 1437–1449
43. Lazo, P. A. (2007) *Cancer Sci.* **98,** 1666–1677
44. Foster, L. J., De Hoog, C. L., and Mann, M. (2003) *Proc. Natl. Acad. Sci. U.S.A.* **100,** 5813–5818
45. Blonder, J., Hale, M. L., Lucas, D. A., Schaefer, C. F., Yu, L. R., Conrads, T. P., Issaq, H. J., Stiles, B. G., and Veenstra, T. D. (2004) *Electrophoresis* **25,** 1307–1318
46. McMahon, K. A., Zhu, M., Kwon, S. W., Liu, P., Zhao, Y., and Anderson, R. G. (2006) *Proteomics* **6,** 143–152
47. Berditchevski, F., Gilbert, E., Griffiths, M. R., Fitter, S., Ashman, L., and Jenner, S. J. (2001) *J. Biol. Chem.* **276,** 41165–41174
48. Yang, X., Claas, C., Kraeft, S. K., Chen, L. B., Wang, Z., Kreidberg, J. A., and Hemler, M. E. (2002) *Mol. Biol. Cell* **13,** 767–781
49. Berditchevski, F., Odintsova, E., Sawada, S., and Gilbert, E. (2002) *J. Biol. Chem.* **277,** 36991–37000
50. Charrin, S., Manié, S., Oualid, M., Billard, M., Boucheix, C., and Rubinstein, E. (2002) *FEBS Lett.* **516,** 139–144
51. Udovichenko, I. P., Gibbs, D., and Williams, D. S. (2002) *J. Cell Sci.* **115,** 445–450
52. Inoue, A., and Ikebe, M. (2003) *J. Biol. Chem.* **278,** 5478–5487
53. Mburu, P., Kikkawa, Y., Townsend, S., Romero, R., Yonekawa, H., and Brown, S. D. (2006) *Proc. Natl. Acad. Sci. U.S.A.* **103,** 10973–10978
54. Nachury, M. V., Loktev, A. V., Zhang, Q., Westlake, C. J., Peränen, J., Merdes, A., Slusarski, D. C., Scheller, R. H., Bazan, J. F., Sheffield, V. C., and Jackson, P. K. (2007) *Cell* **129,** 1201–1213
55. Tusnády, G. E., and Simon, I. (2001) *Bioinformatics* **17,** 849–850
56. Geng, R., Geller, S. F., Hayashi, T., Ray, C. A., Reh, T. A., Bermingham-McDonogh, O., Jones, S. M., Wright, C. G., Melki, S., Imanishi, Y., Palczewski, K., Alagramam, K. N., and Flannery, J. G. (May 3, 2009) *Hum. Mol. Genet.* 10.1093/hmg/ddp210